Hindawi
Journal of Sensors
Volume 2020, Article ID 8815622, 13 pages
https://doi.org/10.1155/2020/8815622

Research Article

Achieving Millimetre Wave Seeker Performance Evaluation Based on the Real-Time Kinematic

Shichao Chen,[1] Fugang Lu,[1] Ming Liu,[2] Jingbiao Wei,[3] and Mengdao Xing[4]

[1]*No. 203 Research Institute of China Ordnance Industries, Xi'an 710065, China*
[2]*School of Computer Science, Shaanxi Normal University, Xi'an 710119, China*
[3]*Army Aviation Research Institute, Beijing 101121, China*
[4]*National Laboratory of Radar Signal Processing, Xidian University, Xi'an 710071, China*

Correspondence should be addressed to Ming Liu; mliu@snnu.edu.cn

Received 10 June 2020; Revised 29 November 2020; Accepted 10 December 2020; Published 24 December 2020

Academic Editor: Antonio Martinez-Olmos

The millimetre wave (MMW) seeker can realize target detection under all weather conditions, the performance of which directly determines the design of the control algorithms. To guarantee the hitting accuracy and damaging effect of the expensive MMW guidance missile, assessing the performance of the seeker is indispensable before the launching of the missile. Real tactical environment of the seeker cannot be simulated comprehensively by indoor laboratories, and high-precision evaluation method outdoor is desperately needed. Focusing on the problem, a method for outdoor MMW seeker performance evaluation is proposed via the real-time kinematic (RTK) technology in this paper, which has the advantages of high-precision orientation and working ability under all climates. Firstly, the geometry of the seeker performance evaluation system is constructed, guaranteeing the effective working of the RTK. And then, the key parameters associated with the guidance control are calculated on the basis of the global position system (GPS) measurements. Finally, comparisons are made between the parameters obtained based on the RTK and the seeker outputs. Besides, for the performance assessment of the MMW seeker towards moving targets, a time synchronization method for different GPS carrier platforms is presented. The effectiveness of the proposed method is validated by the mooring test-fly experiments. Experimental results demonstrate that the performance of the MMW seeker can be evaluated effectively by using the proposed RTK-based method.

1. Introduction

Different from laser seekers [1, 2] or imaging seekers (including television seekers [3] and infrared seekers [4, 5]), the radar seeker is an active homing guidance sensor. It steers itself onto the target by sensing radar cross scatterings [6, 7] and realize "fire and forget" [8] for the missile, which greatly enhances the safety of the launching platforms and the aviators. Moreover, it can be used day and night under various severe environments and climates. And the millimetre wave (MMW) seeker has been the most popular choice among all the radar seekers due to various factors such as the atmospheric attenuation and constraints between the working range and the weight [9, 10].

The precision of the key parameters of the seeker plays a crucial role in the designing of the control algorithms [11, 12]. For example, an accurate line-of-sight (LOS) angular rate of the seeker is the precondition of the precise proportional navigation guidance. However, due to the existence of various nonideal factors, such as the sensitivity to radome slope, missile acceleration, and noises, the LOS angular rates of the seeker cannot be as accurate as the results that are theoretically calculated. Therefore, how to evaluate the precision of the parameters of the MMW seeker is quite important. Firstly, the performance of the MMW seeker needs to be tested in indoor laboratories like microwaves anechoic chambers. In indoor laboratories, the parameters of the MMW seeker can be tested, such as size, weight, dynamic response time, and precision of the LOS angular rates with target simulators. The MMW seeker is mounted on a three-dimensional (3-D) turntable, and the target simulator is mounted on a two-dimensional (2-D) translational system.

The simulation computer will send various kinds of signals or instructions to the MMW seeker and the 3-D turntable and the 2-D translational system for different parameter testing. To better simulate the missile's practical environments, we also need to evaluate the performance of the MMW seeker outdoors.

To realize accurate evaluation of the MMW seeker, we need to know the precise positions of the seeker and the interested target. In other words, we have to provide the basis or standard value for the MMW seeker testing. In the existing literatures, methods about simulation systems or array designing for air-to-air MMW seeker have been presented [13, 14]. A combined guidance method fusing MMW and infrared is proposed in [15]. However, research related to MMW seeker performance evaluation is relatively rare. Motivated by the advantages of short measurement and high precision of the real-time kinematic (RTK) technology [16–18], an evaluation method to realize accurate performance evaluation of the MMW seeker is proposed in this paper. We mount the MMW seeker on a flyable platform which can simulate the missile's trajectory to construct the evaluation system. And an effective performance evaluation method which can test various capabilities of the seeker, such as capturing, tracking, and recapturing, is presented. During the flight, the seeker will output the information that is useful for the terminal guidance, and we will evaluate the precision of these parameters. Making use of the geometry relationships of the target and the seeker and utilizing some mathematic skills, we can calculate the key parameters of the MMW seeker. The performance of the MMW seeker can be evaluated by comparing the parameters obtained from different sources.

2. Principle of the RTK Technology

In the beginning, we will give a brief introduction of the RTK technology. The positioning accuracy of the RTK is within centimetres. It can work smoothly without the influence of barriers. The errors of the measurement are not accumulated [16–18].

Assuming that the coordinates of the satellite and the checking location are (x_s, y_s, z_s) and (x, y, z), respectively, using the formula between two points, we have

$$d = \sqrt{(x - x_s)^2 + (y - y_s)^2 + (z - z_s)^2}. \quad (1)$$

Since the coordinate of the satellite (x_s, y_s, z_s) can be obtained by the navigation message of the satellite, so the unknown parameters in (1) are x, y, and z. If the receiver receives signals from three or more than three satellites, we will have

$$\left.\begin{aligned} d_1 &= \sqrt{(x - x_{s1})^2 + (y - y_{s1})^2 + (z - z_{s1})^2} \\ d_2 &= \sqrt{(x - x_{s1})^2 + (y - y_{s1})^2 + (z - z_{s1})^2} \\ &\cdots, \\ d_N &= \sqrt{(x - x_{sN})^2 + (y - y_{sN})^2 + (z - z_{sN})^2} \end{aligned}\right\}, \quad (2)$$

where d_i is the distance from the $i^{\text{th}} (i = 1, 2, \cdots, N)$ satellite to (x, y, z). (x_{si}, y_{si}, z_{si}) is the coordinate of the i^{th} satellite, and $N (N \geq 3)$ is the total number of the satellites. As can be seen, as long as N is greater than 3, we can get the coordinate of (x, y, z) by solving (2). Actually, we need another equation to solve the coordinate due to the existence of satellite clock error [19, 20], which will not be detailed discussed here.

However, what we get in this way is the pseudorange, which includes various errors. The precision can only reach meters under this condition, which limits the application. As a result, more than two global position system (GPS) [19, 20] receivers are utilized in the RTK system to eliminate the errors. One receiver is mounted on a predefined location as the reference, whereas other receivers are used as the mobile stations to test the interested locations. Owing to the merit that the pseudoranges are obtained both for the reference position and the checking position, the system error can be regarded to be the same within some measurement range. The filtered coordinate of the reference point subtracted by the precise coordinate comes out to be the total system error. Through the radio communication between the reference point and the checking point, the total system error is real-time transported to the checking point, and the coordinate of the checking point can be corrected subsequently. The system can provide the positioning precision of as high as centimetres. The main working principle of the RTK is displayed in Figure 1.

3. Parameter Calculation Based on RTK

3.1. Configuration Construction. To realize accurate performance evaluation of the MMW seeker, we firstly construct the working system of the RTK. We mount the MMW seeker on a moving platform such as a helicopter or an unmanned aerial vehicle (UAV) and combine the inertial navigation system (INS) and the missile-borne computer together to form the MMW seeker evaluation system. The constructed geometry is demonstrated in Figure 2. According to the simulated digital ballistic trajectory of the missile, we design the track of the flyable platform and the positions of the main station and the substations of the RTK system, guaranteeing the main station and the substations to work within the effective range of the RTK. Three GPS receivers are used in the evaluation system. The reference station is predefined. One of the rover receivers is installed on the helicopter, which carries the MMW seeker. And the other rover receiver is installed on the target. The platform carrying the MMW seeker flies towards the interested target according to the digital simulated trajectory, and the MMW seeker will start to illuminate electromagnetic wave to interested areas to detect the target when the distance from the seeker and the target is within the effective working range of the MMW seeker. The pointing directions of the seeker can be provided by the missile-borne computer to improve target-capturing probability [10].

During the flight, the GPS receiver on the moving platform will record the coordinates of the seeker in real time. At the meantime, the GPS receiver on the target will also record the position of the target. Generally, the effective

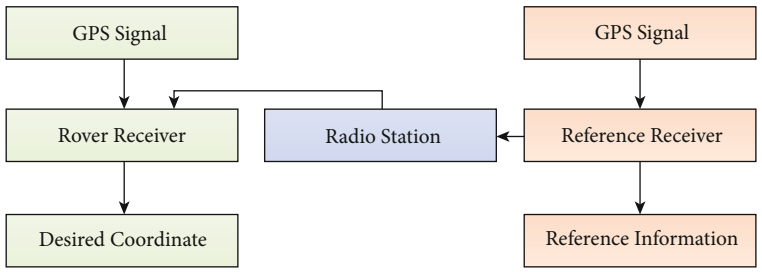

Figure 1: Working principle of RTK.

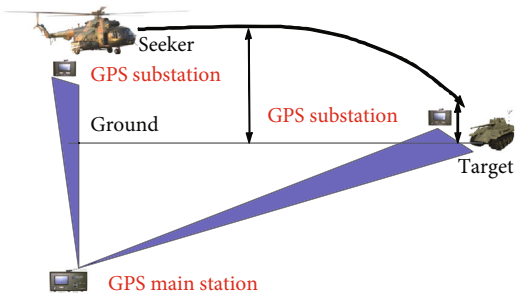

Figure 2: Geometry configuration of the RTK-based evaluation system.

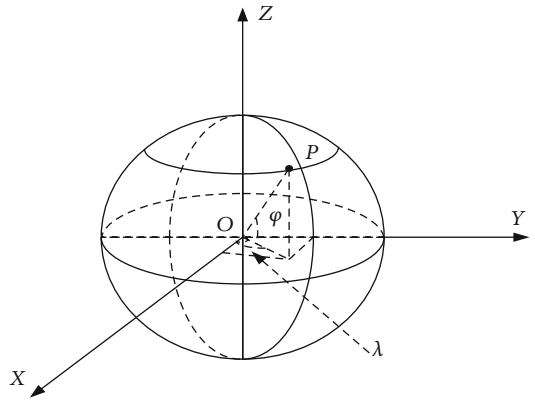

Figure 3: Diagram of the coordinate system associated with meridian plane.

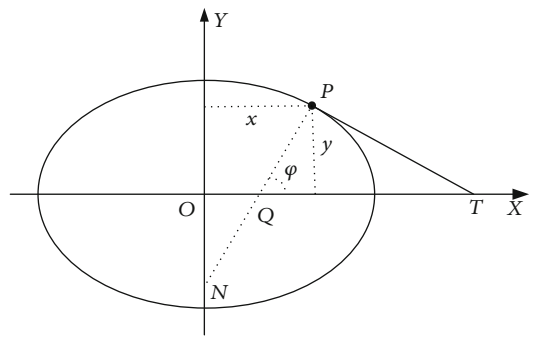

Figure 4: Geometric relationship of the *POZ* plane.

working range of the RTK is about 4 km. Fortunately, for the helicopter-borne or UAV-borne air-to-ground missile (AGM) discussed in this paper, the effective working range of the MMW seeker is less than 4 km. Therefore, the constructed evaluation configuration can ensure the positioning accuracy of the RTK.

Parameters associated with the MMW seeker can be calculated based on the recorded positions of the seeker and the targets, such as the seeker to target distance and the LOS angular rates in the pitching and yawing directions. Making comparisons between these parameters with the ones outputted by the MMW seeker itself, the real-time evaluation of the MMW seeker can be realized.

3.2. Parameter Calculation. Supposing that the earth is an ellipsoid, as shown in Figure 3, the intersection of the prime meridian plane and the equatorial plane forms the X axis, the direction perpendicular to the X axis on the equatorial plane is the Y axis, and the Z axis, X axis, and Y axis constitute the right-handed coordinate system. P represents any point on the earth's surface, λ represents the longitude, and φ represents the latitude. The parameters can be obtained by the GPS receivers in real time. Extracting the meridian plane from point P, we can get the Cartesian coordinate system, as shown in Figure 4.

Firstly, make the tangent line PT through point P, and the first-order derivative at point P is the tangent of the angle $\angle PTX$ based on the analytic geometry.

$$\frac{dy}{dx} = \tan\angle PTX = \tan\left(90^\circ + \varphi\right) = -\cot\varphi. \tag{3}$$

Since point P lies on the ellipse and according to the elliptic equation, we have

$$\frac{x^2}{a^2} + \frac{y^2}{b^2} = 1, \tag{4}$$

where a is the semimajor axis, and b is the semiminor axis [21]. Making the first-order deviation to (4) with respect to x, we have

$$\frac{dy}{dx} = -\frac{b^2}{a^2} \bullet \frac{x}{y}. \tag{5}$$

Combining (3) and (5) together, we have

$$\cot\varphi = \frac{b^2}{a^2} \bullet \frac{x}{y} = \frac{a^2 - c^2}{a^2} \bullet \frac{x}{y} = \left(1 - e^2\right) \bullet \frac{x}{y}, \tag{6}$$

where c represents the focus of the ellipse, and $e = \sqrt{(a^2 - b^2)/a^2}$ is the eccentricity ratio. From (6), we have

$$y = x\left(1 - e^2\right) \tan\varphi. \tag{7}$$

Substituting (7) into (4), we have

$$\frac{x^2}{a^2} + \frac{x^2\left(1 - e^2\right)^2 \tan^2\varphi}{b^2} = 1. \tag{8}$$

Multiplying both sides of (8) by $a^2 \cos^2\varphi$, we have

$$x^2\left(1 - e^2 \sin^2\varphi\right) = a^2 \cos^2\varphi. \tag{9}$$

Detailed deduction from (8) to (9) is given in Appendix. Or better, we have

$$x = \frac{a \cos\varphi}{\sqrt{1 - e^2 \sin^2\varphi}}. \tag{10}$$

Substituting (10) into (7), we have

$$y = \frac{a\left(1 - e^2\right) \sin\varphi}{\sqrt{1 - e^2 \sin^2\varphi}}. \tag{11}$$

According to the geometry relationships of Figures 3 and 4, the spatial rectangular coordinate of the target position can be expressed as

$$\left.\begin{aligned} X &= x \cdot \cos\lambda \\ Y &= x \cdot \sin\lambda \\ Z &= y \end{aligned}\right\}. \tag{12}$$

Let $N = a/\sqrt{1 - e^2 \sin^2(\varphi)}$, and combine (10) and (11), and (12) can be updated by

$$\left.\begin{aligned} X &= N \cdot \cos\varphi \cdot \cos\lambda \\ Y &= N \cdot \cos\varphi \cdot \sin\lambda \\ Z &= N \cdot \left(1 - e^2\right) \cdot \sin\varphi \end{aligned}\right\}. \tag{13}$$

If point P is not on the surface of the earth and supposing the corresponding height is h, the Cartesian coordinate position of the target will be

$$\left.\begin{aligned} X &= (N + h) \cdot \cos\varphi \cdot \cos\lambda \\ Y &= (N + h) \cdot \cos\varphi \cdot \sin\lambda \\ Z &= \left[N \cdot \left(1 - e^2\right) + h\right] \cdot \cos\varphi \end{aligned}\right\}. \tag{14}$$

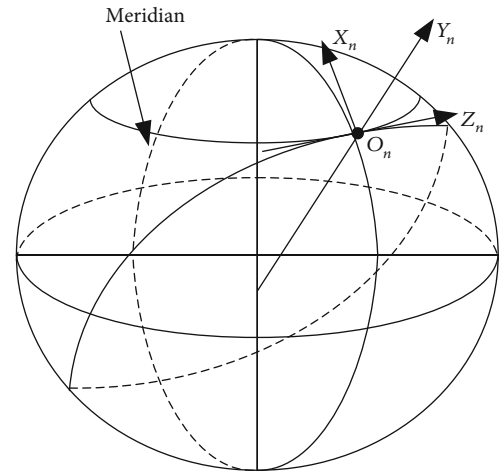

Figure 5: Diagram of the coordinate system.

Hereto, we can get the rectangular coordinates of the target and the MMW seeker, respectively. The position of the target is

$$\left.\begin{aligned} x_t &= (N_t + h_t) \cdot \cos\varphi_t \cos\lambda_t \\ y_t &= (N_t + h_t) \cdot \cos\varphi_t \cdot \sin\lambda_t \\ z_t &= \left[N_t\left(1 - e^2\right) + h_t\right] \cdot \sin\varphi_t \end{aligned}\right\}. \tag{15}$$

And the position of the seeker is

$$\left.\begin{aligned} x_a &= (N_a + h_a) \cdot \cos(\lambda_a) \cdot \cos(\varphi_a) \\ y_a &= (N_a + h_a) \cdot \sin(\lambda_a) \cdot \cos(\varphi_a) \\ z_a &= \left[N_a\left(1 - e^2\right) + h_a\right] \cdot \sin(\varphi_a) \end{aligned}\right\}, \tag{16}$$

where $N_a = a/\sqrt{1 - e^2 \sin^2(\varphi_a)}$, and $N_t = a/\sqrt{1 - e^2 \sin^2(\varphi_t)}$. The subscripts t and a stand for the target and the seeker, respectively.

What follows is to transform the coordinate into the navigation coordinates (x_T, y_T, z_T), as shown in Figure 5.

To realize the transformation, we first make the Cartesian coordinate system $OXYZ$ rotate λ_a radians around the Z axis to get $OX'Y'Z'$, as shown in Figure 6(a). The relationships between coordinate systems $OXYZ$ and $OX'Y'Z'$ can be expressed as

$$\begin{bmatrix} x' \\ y' \\ z' \end{bmatrix} = L(\lambda_a) \begin{bmatrix} x_t - x_a \\ y_t - y_a \\ z_t - z_a \end{bmatrix}, \tag{17}$$

where

$$L(\lambda_a) = \begin{bmatrix} \cos\lambda_a & \sin\lambda_a & 0 \\ -\sin\lambda_a & \cos\lambda_a & 0 \\ 0 & 0 & 1 \end{bmatrix}. \tag{18}$$

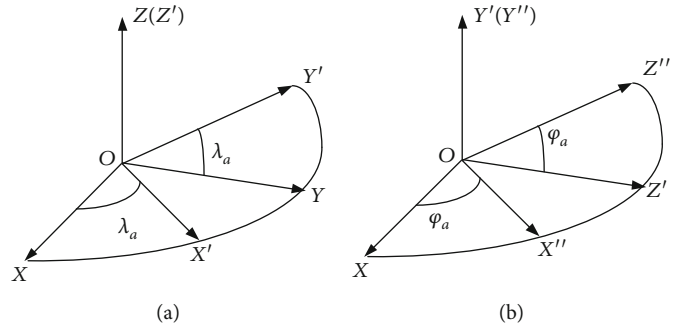

FIGURE 6: Illustration of the rotation from the rectangular coordinate system to the navigation coordinate system. (a) The first rotation. (b) The second rotation.

Rotating φ_a radians around Y' axis, we can obtain $OX''Y''Z''$. The corresponding rotation is shown in Figure 6(b). The relationships between the coordinate systems of $OX'Y'Z'$ and $OX''Y''Z''$ can be expressed as

$$\begin{bmatrix} x'' \\ y'' \\ z'' \end{bmatrix} = L(\varphi_a) \begin{bmatrix} x' \\ y' \\ z' \end{bmatrix}, \tag{19}$$

where

$$L(\varphi_a) = \begin{bmatrix} \cos\varphi_a & 0 & \sin\varphi_a \\ 0 & 1 & 0 \\ -\sin\varphi_a & 0 & \cos\varphi_a \end{bmatrix}. \tag{20}$$

However, we still cannot realize the complete transformation of the coordinates by far, since the rotated axes of $OX''Y''Z''$ cannot exactly correspond to the axes of $OX_NY_NZ_N$. From the comparison between Figures 3 and 5, we can see that OZ'' corresponds to OX_N, OY'' corresponds to OZ_N, and OX'' corresponds to OY_N. That is to say, we still need to multiply the result by the following rotation matrix $\mathbf{E}$ to obtain the final navigation coordinate.

$$\mathbf{E} = \begin{bmatrix} 0 & 0 & 1 \\ 1 & 0 & 0 \\ 0 & 1 & 0 \end{bmatrix}. \tag{21}$$

To summarize, the whole transformation matrix can be expressed as

$$\begin{aligned} L(\varphi_a, \lambda_a) &= \mathbf{E} \bullet L(\varphi_a) \bullet L(\lambda_a) \\ &= \begin{bmatrix} -\sin\varphi_a\cos\lambda_a & -\sin\varphi_a\sin\lambda_a & \cos\varphi_a \\ \cos\varphi_a\cos\lambda_a & \cos\varphi_a\sin\lambda_a & \sin\varphi_a \\ -\sin\lambda_a & \cos\lambda_a & 0 \end{bmatrix}, \end{aligned} \tag{22}$$

And the whole rotation process is shown in Figure 7.

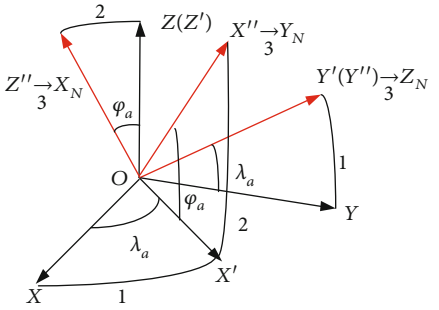

FIGURE 7: Illustration of the whole rotation process.

Transforming the coordinate into the navigation coordinate by using $L(\varphi_a, \lambda_a)$, the coordinate arrives at (x_T, y_T, z_T).

$$\begin{bmatrix} x_T \\ y_T \\ z_T \end{bmatrix} = \begin{bmatrix} -\sin\varphi_a\cos\lambda_a & -\sin\varphi_a\sin\lambda_a & \cos\varphi_a \\ \cos\varphi_a\cos\lambda_a & \cos\varphi_a\sin\lambda_a & \sin\varphi_a \\ -\sin\varphi_a & \cos\lambda_a & 0 \end{bmatrix} \begin{bmatrix} x_t' \\ y_t' \\ z_t' \end{bmatrix}. \tag{23}$$

Hereto, we can calculate the seeker to target distance.

$$d_{\mathrm{TA}} = \sqrt{x_T^2 + y_T^2 + z_T^2}. \tag{24}$$

Assuming that there is no rolling during the flight of the seeker, the pitching angle θ_{n0} and the yawing angle φ_{n0} can be calculated according to the geometry relationship between the target and the seeker, as shown in Figure 8.

$$\begin{aligned} \theta_{n0} &= \arctan\left(\frac{y_T}{\sqrt{x_T^2 + z_T^2}}\right), \\ \varphi_{n0} &= \arctan\left(\frac{z_T}{x_T}\right). \end{aligned} \tag{25}$$

Differentiating θ_{n0} and φ_{n0}, we can get the pitching LOS angular rate $\dot{\theta}_{n0}$ and the yawing LOS angular rate $\dot{\varphi}_{n0}$. Comparing the calculated parameters with the ones outputted by the MMW seeker, we can evaluate the performance of the seeker.

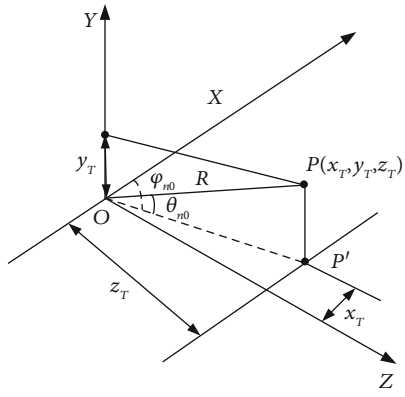

Figure 8: Relationships of the pitching and yawing angles.

3.3. Parameter Error Analysis. In this part, we come to discuss the influences of the measurement errors of the GPS on the parameters, taking a helicopter-borne AGM whose firing range is 10 km for an illustration. The MMW seeker starts to work with seeker to target distance 2.5 km, and it moves towards the target from far to near according to the simulated missile trajectory. However, the presented mooring test-fly experiment cannot realize the simulation of the missile's whole trajectory due to various factors. Firstly, when the seeker to target distance is less than the blind zone of the radar, parameters will not be outputted by the seeker. Therefore, parameters correspond to the blind zone of the radar are not necessary. Besides, to guarantee the security of the moving platform, the platform will not approach the target indefinitely like the missiles. A safety distance must be guaranteed, and we set the safety flying height of the helicopter to be the threshold in the experiment. When the height of the helicopter approaches 40 m, the aviator will pull up the helicopter. The effective working range of x_T and y_T is given in Figure 9. Since the RTK GPS can achieve centimetre accuracy, we conduct simulations with an assumption that the RTK errors range from 2 cm to 10 cm based on real parameters by using the Matlab software.

3.3.1. Seeker to Target Distance. The seeker to target distance can be updated by

$$d_{\mathrm{TA}} = \sqrt{(x_T + \Delta x_T)^2 + (y_T + \Delta y_T)^2 + (z_T + \Delta z_T)^2}. \quad (26)$$

Δx_T, Δy_T, and Δz_T represent the GPS measurement errors along the three directions, respectively. Making Taylor series expansion with respect to d_{TA}, we have

$$d_{\mathrm{TA}} = d_{\mathrm{TA0}} + \Delta d_{\mathrm{TA0}}, \quad (27)$$

where

$$\Delta d_{\mathrm{TA0}} = \frac{x_T \Delta x_T}{\sqrt{x_T^2 + y_T^2}} + \frac{y_T \Delta y_T}{\sqrt{x_T^2 + y_T^2}}. \quad (28)$$

The influences on the precision of d_{TA} caused by the GPS measurement errors are shown in Figure 10. As can be seen, when the error increases from 2 cm to 10 cm, the influence becomes larger gradually. Even when the measurement error reaches 10 cm, the maximum distance error is still less than 0.1 m. The error is totally intolerable for the active homing MMW seeker.

3.3.2. LOS Angles. In the following, we come to see the LOS angles. The pitching angle with the consideration of measurement errors will be

$$\theta_n = \arctan\left[\frac{(y_T + \Delta y_T)}{\sqrt{(x_T + \Delta x_T)^2 + (z_T + \Delta z_T)^2}}\right]. \quad (29)$$

Still making Taylor series expansion, we have

$$\theta_n = \theta_{n0} + \Delta\theta_n, \quad (30)$$

where

$$\Delta\theta_n = \frac{-y_T \Delta x_T}{(x_T^2 + y_T^2)} + \frac{x_T \Delta y_T}{(x_T^2 + y_T^2)}. \quad (31)$$

Similarly, the yawing angle with the involved error can be updated by

$$\varphi_n = \arctan\left[\frac{(z_T + \Delta z_T)}{(x_T + \Delta x_T)}\right]. \quad (32)$$

Implementing the same process as the pitching angle, we have

$$\varphi_n = \varphi_{n0} + \Delta\varphi_n, \quad (33)$$

where

$$\Delta\varphi_n = \frac{\Delta z_T}{x_T}. \quad (34)$$

The errors of the pitching LOS angle caused by the GPS measurements are shown in Figure 11, and the influences on the precision of the yawing LOS angle are shown in Figure 12. As can be seen, the error of the pitching angle and the yaw angle are around 10^{-4} and 10^{-5} radians; the influence is small enough to neglect for active homing guidance. As a result, the influence caused by GPS measurements on LOS angular rates can also be neglected.

4. Experiments and Analysis

4.1. Evaluation of the MMW Seeker towards Stationary Targets. The effectiveness of the proposed algorithm is verified on the real collected data by the mooring test-fly experiment. Since the RTK GPS plays the role of the baseline, it is the precondition of the whole performance evaluation of the MMW seeker. As a result, to realize better performance of the RTK GPS, the mooring test-fly experiment needs to be conducted on open and vast space many times to

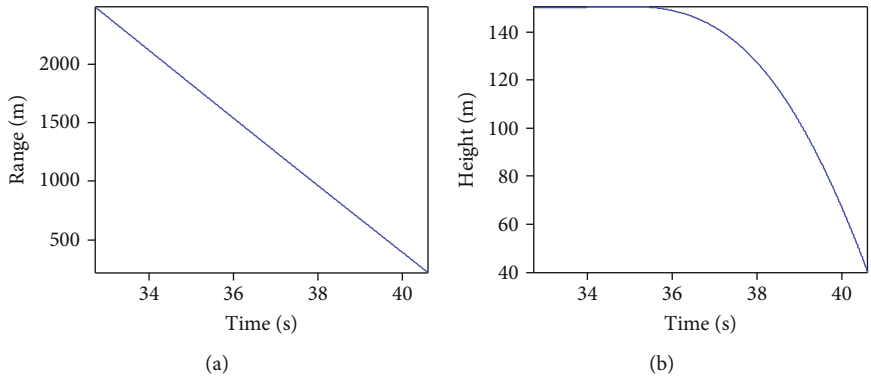

Figure 9: Effective terminal trajectory of the seeker. (a) Along the X direction. (b) Along the Y direction.

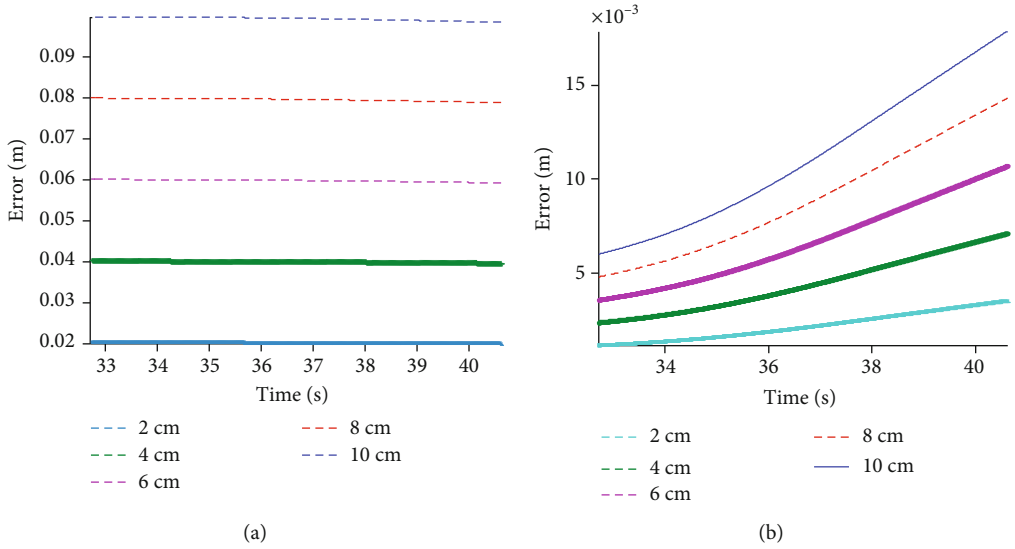

Figure 10: The errors of the seeker to target distance caused by the GPS measurements. (a) Along the X direction. (b) Along the Y direction.

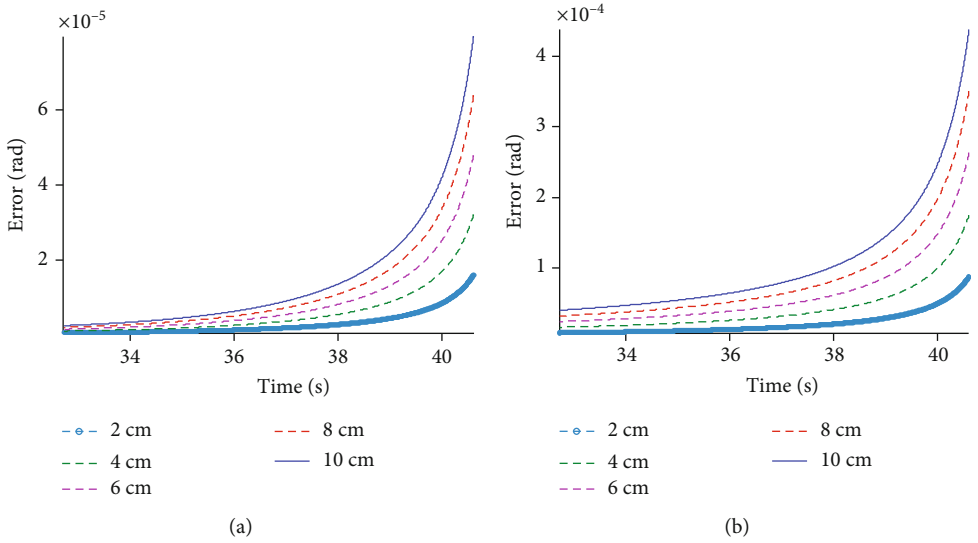

Figure 11: The errors of the pitching LOS angle caused by GPS measurements. (a) Along the X direction. (b) Along the Y direction.

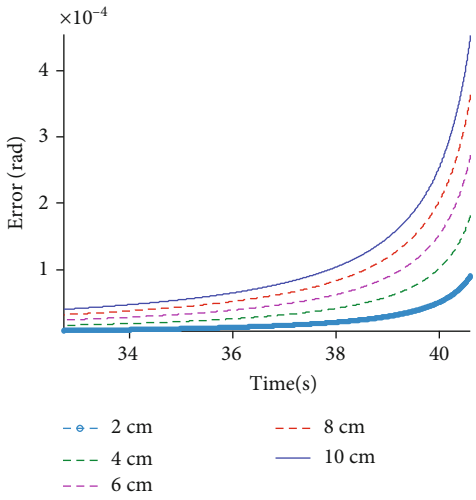

Figure 12: The errors of the yawing LOS angle caused by GPS measurements.

guarantee the satellite signal receiving quality. The tested MMW seeker is used for land threatening targets attacking, whose resolution is 6 m in range. And the brand of the RTK GPS is LD-VB50F for the reference station, and LD-VR50F is for the substations provided by a Chinese company.

We test the proposed method on evaluations towards stationary targets and moving targets, respectively. We test the performance of the proposed method on stationary targets first. The evaluation system is constructed as follows: the reference station is stabilized on a precise located position, and the substations are mounted on the helicopter with an MMW seeker and the target, respectively. The platform simulates the ballistic trajectory during flying, guaranteeing that the RTK system works within its effective working radius. The MMW seeker starts to illuminate electromagnetic wave to detect the target when the seeker to target distance approaches 2.5 km. The interested target is set to be stable in this case. During the process, the parameters are calculated by using the proposed RTK-based method. At the meantime, the MMW seeker will also output the associated parameters itself. Results of the seeker to target distance calculated by using the proposed method and outputted by the MMW seeker are shown in Figure 13. Corresponding results of the pitching LOS angular rate and yawing LOS angular rate are demonstrated in Figures 14 and 15, respectively. Local enlarging results are also provided. Inspecting Figure 14(a), we can see that there is a spike in the seeker's output. This is caused by the target recapture of the MMW seeker. From the output of the RTK, we can see that the mismatching between the seeker's output and the RTK-based method is explicit, based on which, we can evaluate the performance of the tested MMW seeker. The phenomenon further demonstrates the effectiveness of the proposed method.

As can be seen from Figures 13–15, the results obtained by using the proposed RTK-based method correspond to the seeker's outputs. The calculated parameters can accurately reflect the performance of the MMW seeker. The error of the seeker to target distance is less than 3 m, the error of the pitching LOS angular rate is about 0.1°, and the error of the yawing LOS angular rate is about 0.4°. To further verify the effectiveness of the proposed method, comparisons between the proposed RTK-based method and the INS information-based method are conducted. The reason why we compare the proposed method with the INS information-based one is that using INS is an intuitive and cost-effective way of evaluating the MMW seeker (the INS system belongs to the whole weapon system). Taking the LOS angular rates as an illustration, results of the yawing LOS angular rate and the pitching LOS angular rate under the two different methods are given in Figure 16. As can be seen, the performance of the INS information-based method is much worse than the proposed RTK-based one, especially for the pitching direction. The error caused by the INS is intolerable, the reason lies in the fact that the drifting error and jumping error of the INS happen much more frequently. Besides, the accumulated error will get larger with the increasing of the time for the INS [22, 23]. The INS information-based method is not appropriate for the long-time testing of the MMW seeker.

4.2. Evaluation of the MMW Seeker towards Moving Targets. In this part, we come to test the proposed method on a moving target case; the MMW seeker will illuminate a moving target in this case. Different from the stationary case, for moving targets, we need to realize time synchronization first.

The time clocks of the MMW seeker and the rover receivers located on different platforms are not the same during the flight. A time synchronization method is proposed to solve the problem. The time clock of the centre control of the evaluation system is regarded as the reference, and the synchronization time of the devices are initialized as t_0, t_1, and t_2, respectively. T_1 and T_2 represent the time sequences of the rover receivers, and $t_{1\mathrm{GPS}}$ and $t_{2\mathrm{GPS}}$ represent the GPS time [24, 25] sequences of the rover receivers, respectively. The process of the proposed time synchronization method is given in Figure 17. The synchronization process consists of two main parts. The first part is to synchronize t_0 with t_1 by traversing the time sequence of T_1. The terminal condition is to determine the data sampling interval T_0. And the second part is to synchronize t_1 with t_2 by traversing the time sequence of T_2. The terminal condition of this part is to determine the GPS time interval T_{GPS} between the rover receivers.

After time synchronization, the key parameters of the MMW seeker are calculated with the GPS measurements by using the proposed method. And then, results are compared with the ones outputted by the seeker to evaluate the performance of the MMW seeker for the moving targets. Corresponding results are given in Figures 18–20, respectively. Similarly, corresponding local enlarging results are also displayed accordingly. As can be seen from the results, the difference of the seeker to target distance is less than 3 m, and the difference of the pitching LOS angular rate is less than 0.15°, and the difference in the yawing direction is less than 0.2° in this case. The results shown here are well enough for the terminal control of the active homing MMW guidance helicopter-borne AGM.

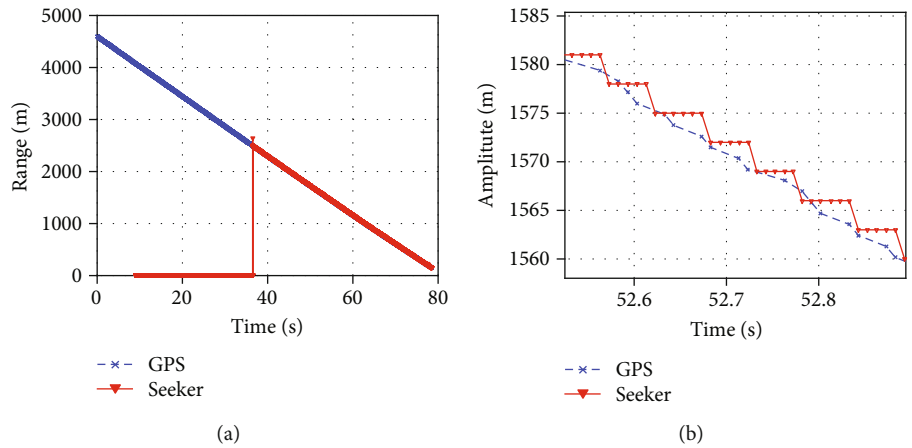

Figure 13: Results of the seeker to target distance. (a) Total flight. (b) Local enlarging results.

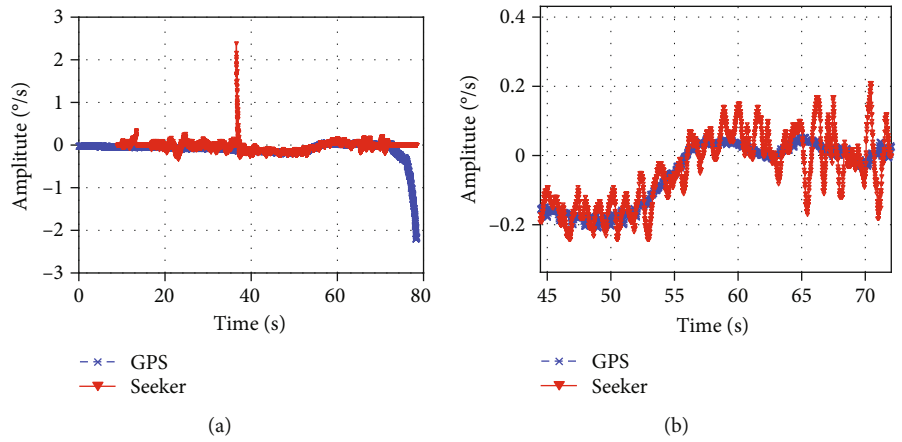

Figure 14: Results of the pitching LOS angular rate. (a) Total flight. (b) Local enlarging results.

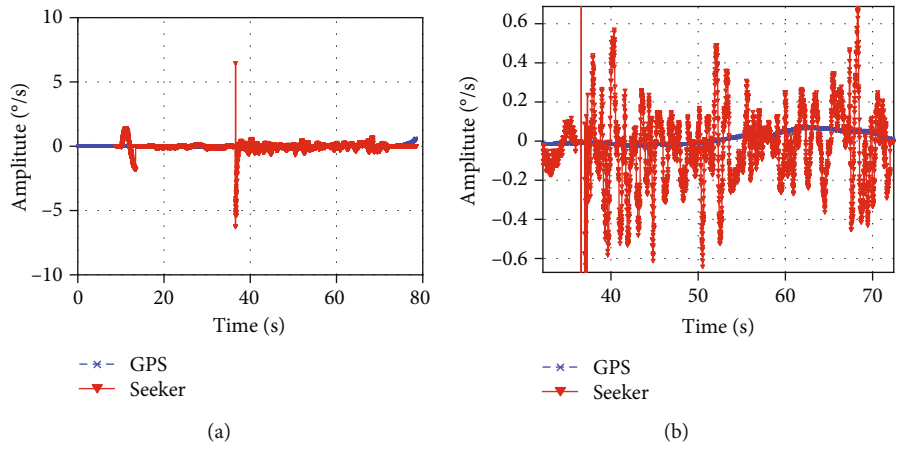

Figure 15: Results of the yawing LOS angular rate. (a) Total flight. (b) Local enlarging results.

From the experimental results, we can see that the measuring error (the error between the seeker's output and the proposed method) in range is less than half of the range resolution of the MMW seeker. The error is acceptable for MMW seeker performance evaluation. In practice, we set the detected value of a given resolution cell to be the middle value. In Figure 21, we demonstrate the measuring error with respect to the range resolution of the MMW seeker,

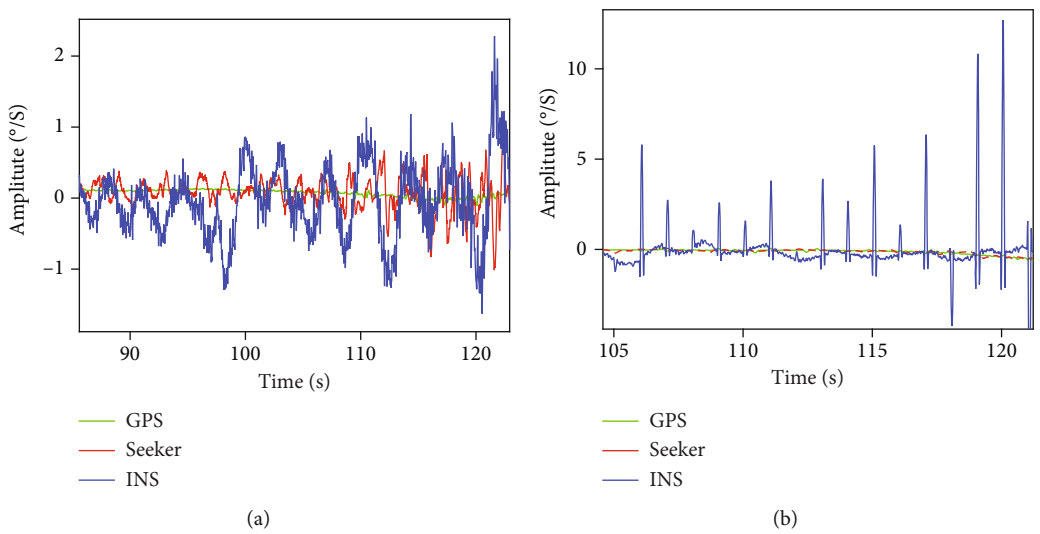

Figure 16: Comparisons between the INS and RTK-based methods. (a) Yawing LOS angular rate. (b) Pitching LOS angular rate.

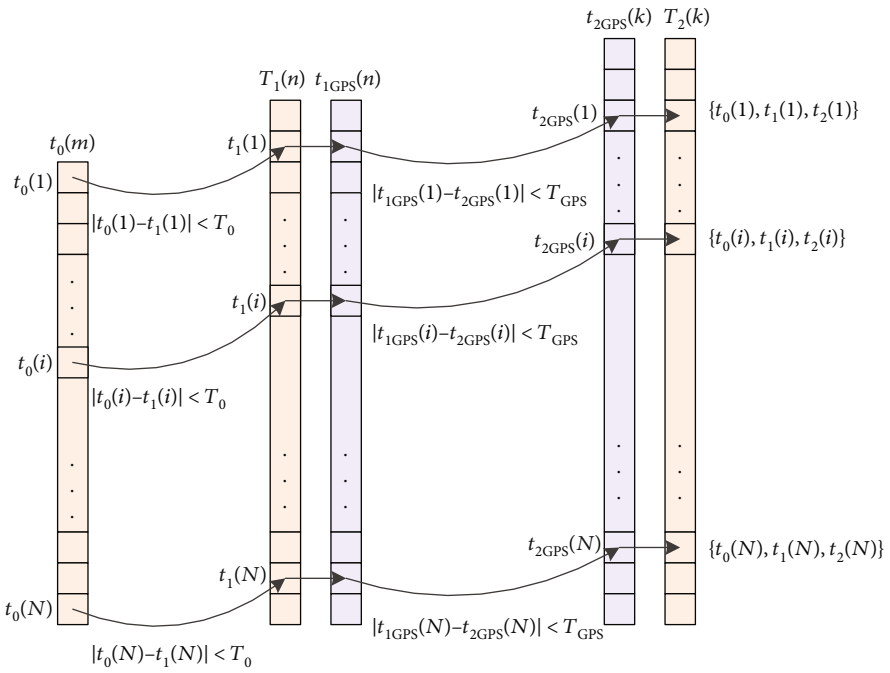

Figure 17: Process of the time synchronization.

supposing that $|AB|$ represents the length of the range resolution ρ_r. If the detected range of the MMW seeker lies within the scope of $|AB|$, e.g., $R_i(i = 1, 2, \cdots, N)$, we will view all these positions as the value of point c, and c is the midpoint of $|AB|$. Therefore, the maximum error will be half of the resolution, which is 3 m in this case. That is to say, if the detected distance of the MMW seeker is near point c, the error will be close to zero. If the detected distance is near point A or B, the error will be close to half of the resolution in range.

As for the thresholds of the error of the angular rates along the yawing and pitching directions, they are empirically determined by the semiphysical simulations plenty of times to ensure stable control of the missile body and precise attacking of the threatening targets. In other words, in the semiphysical simulation of the missile system, we will add different level noises to the ideal LOS rates of the MMW seeker to test whether the system works smoothly and whether stable control can be realized. In particular, plenty of collected real data can help to determine the error thresholds.

The errors of the MMW seeker in the experiments are totally tolerable, which satisfies the requirement of precise attacking of the guidance control system of the missile. The proposed method can provide an effective performance evaluation of the MMW seeker.

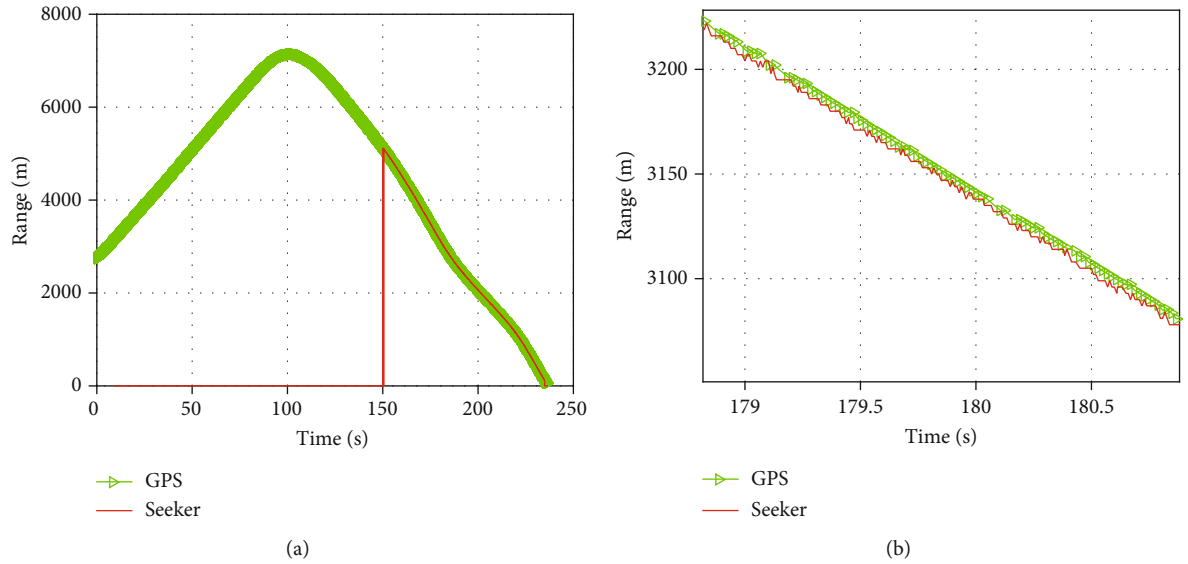

Figure 18: The seeker to target distance. (a) The whole time. (b) Local enlarging results.

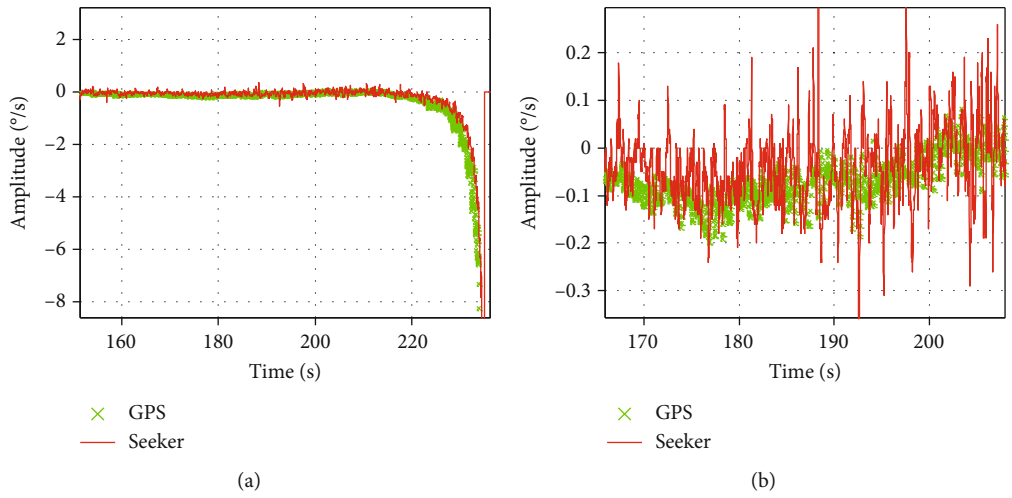

Figure 19: Pitching LOS angular rate. (a) The seeker's working time. (b) Local enlarging results.

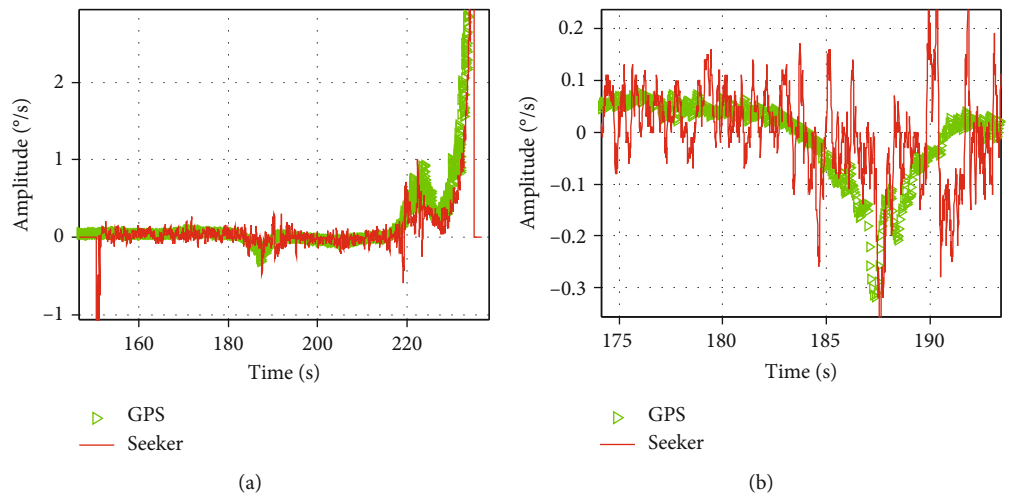

Figure 20: Yawing LOS angular rate. (a) The seeker's working time. (b) Local enlarging results.

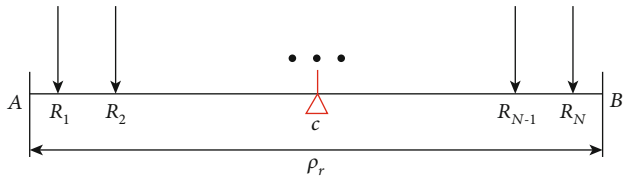

Figure 21: Demonstration of the measuring error with respect to the range resolution of the MMW seeker.

5. Conclusions

An MMW seeker performance evaluation method is proposed via RTK in this paper. By comparing the parameters calculated by using multiple GPS measurements with the ones outputted by the seeker, we can judge the performance of the seeker and guarantee high-precision seeker performance. The influences on the precision of the key parameters of the seeker performance evaluation caused by the GPS measurements are analysed. Mooring test-fly experiments have verified that the proposed method can realize high-precision evaluation of the MMW seeker, which provides the basis of the design of the terminal guidance.

Besides the MMW seeker, the constructed evaluation system and the proposed evaluation method can also be applied into other guidance seekers with necessary modifications.

However, we have to note that the evaluation experiments are all carried out on vast and open space to guarantee the effectiveness of the RTK system. The unfixed coordinate errors from the RTK were not considered in this paper. There may be moments when the RTK GPS may not produce fixed coordinate depending on the quality of the antenna and grade of RTK GPS. This may produce intolerable amount of error and therefore may not be able to provide an accurate reference for the seeker's output. To realize a more effective evaluation of the MMW seeker and improve the efficacy of the experiments, adopting appropriate filtering methods is necessary, which is well worth working on.

Appendix

Detailed Deduction from Equation (8) to Equation (9)

In this part, we give the detail deductions from (A.1) to (A.4).

$$\frac{x^2}{a^2} + \frac{x^2\left(1-e^2\right)^2 \tan^2\varphi}{b^2} = 1. \tag{A.1}$$

Multiplying both sides of (A.1) by $a^2\cos^2\varphi$, we have

$$x^2\cos^2\varphi + \frac{x^2\left(1-e^2\right)^2\tan^2\varphi}{b^2}a^2\cos^2\varphi = a^2\cos^2\varphi \Rightarrow x^2\left[\cos^2\varphi + \frac{a^2\left(1-e^2\right)^2\sin^2\varphi}{b^2}\right] = a^2\cos^2\varphi. \tag{A.2}$$

Substituting $e = \sqrt{(a^2-b^2)/a^2}$ into (A.2), we have

$$\begin{aligned} x^2\left[\cos^2\varphi + \frac{b^2\sin^2\varphi}{a^2}\right] &= a^2\cos^2\varphi \\ \Rightarrow x^2\left[\frac{a^2\cos^2\varphi + b^2\sin^2\varphi}{a^2}\right] &= a^2\cos^2\varphi \\ \Rightarrow x^2\left[\frac{a^2 - a^2\sin^2\varphi + b^2\sin^2\varphi}{a^2}\right] &= a^2\cos^2\varphi \Rightarrow x^2\left[1 - \frac{a^2-b^2}{a^2}\sin^2\varphi\right] \\ &= a^2\cos^2\varphi. \end{aligned} \tag{A.3}$$

Substituting $e = \sqrt{(a^2-b^2)/a^2}$ into (A.3), we have

$$x^2\left[1-e^2\sin^2\varphi\right] = a^2\cos^2\varphi. \tag{A.4}$$

Data Availability

The data used to support the findings of this study are available from the corresponding author upon request.

Conflicts of Interest

The authors declare that there is no conflict of interest regarding the publication of this paper.

Acknowledgments

This work was supported by the National Natural Science Foundation of China (Grant 61701289 and 61601274), the Natural Science Foundation of Shaanxi Province (Grant 2018JQ6083 and 2018JQ6087), the Young Talent Fund of University Association for Science and Technology in Shaanxi (Grant 20190106), and the Fundamental Research Funds for the Central Universities (Grant GK201903084).

References

[1] L. Zhu, F. Jia, X. Jiang, and X. Li, "Photoelectric detection technology of laser seeker signals," *Journal of Systems Engineering and Electronics*, vol. 30, no. 6, pp. 1064–1073, 2019.

[2] Ž. P. Barbarić, M. D. Lutovac, and I. D. Đokić, "Analyses of probability density function of displacement signal for laser seeker systems," in *2011 10th International Conference on Telecommunication in Modern Satellite Cable and Broadcasting Services (TELSIKS)*, pp. 122–125, Nis, Serbia, October 2011.

[3] X.-W. Li, X.-S. Huang, and J.-X. Sun, "Study on strapdown TV seeker simulation method," in *2010 Second International Conference on Computer Modeling and Simulation*, pp. 483–485, Sanya, Hainan, China, January 2010.

[4] M. Polasek, J. Nemecek, and I. Q. Pham, "Counter countermeasure method for missile's imaging infrared seeker," in

2016 IEEE/AIAA 35th Digital Avionics Systems Conference (DASC), pp. 1–8, Sacramento, CA, USA, September 2016.

[5] F. Li, Q. Xia, L. Xiong, and Y. Yao, "Study on air-to-ground missile with strap-down imaging infrared seeker against moving target," in *Proceedings of the 32nd Chinese Control Conference*, pp. 5149–5152, Xi'an, China, July 2013.

[6] S. Han, W. Ra, I. Whang, and J. B. Park, "Geometric joint probabilistic data association approach to ballistic missile warhead tracking using FMCW radar seeker," *IET Radar, Sonar & Navigation*, vol. 10, no. 8, pp. 1422–1430, 2016.

[7] Y. Yang, S. Xiao, D. Feng, and W. Zhang, "Modelling and simulation of spatial-temporal correlated K distributed clutter for coherent radar seeker," *IET Radar, Sonar & Navigation*, vol. 8, no. 1, pp. 1–8, 2014.

[8] J. S. Hunter and J. C. Hung, "Development of low-cost multifunction sensors for lightweight fire and forget antitank weapon system," *IEEE Transactions on Industrial Electronics*, vol. IE-30, no. 1, pp. 1–6, 1983.

[9] J. T. Richard and H. O. Everitt, "Millimeter wave and terahertz synthetic aperture radar for locating metallic scatterers embedded in scattering media," *IEEE Transactions on Terahertz Science and Technology*, vol. 7, no. 6, pp. 732–740, 2017.

[10] F. Lu, S. Chen, M. Liu, J. Wang, F. Ma, and T. Yang, "A target recapturing method for the millimeter wave seeker with narrow beamwidth," in *IGARSS 2018 - 2018 IEEE International Geoscience and Remote Sensing Symposium*, pp. 2841–2844, Valencia, Spain, July 2018.

[11] J. Holloway and M. Krstic, "Predictor observers for proportional navigation systems subjected to seeker delay," *IEEE Transactions on Control Systems Technology*, vol. 24, no. 6, pp. 2002–2015, 2016.

[12] L. Nugroho and A. T. Kutay, "Capturability of combined augmented proportional navigation against a pull-up maneuvering target," in *2015 IEEE International Conference on Aerospace Electronics and Remote Sensing Technology (ICARES)*, pp. 1–9, Bali, Indonesia, December 2015.

[13] L. P. Cecchini, E. Pizzingrilli, S. Russo, and U. F. D'Elia, "MMW active phased array seeker project for hit to kill engagement," in *2008 IEEE Radar Conference*, pp. 1–6, Rome, Italy, May 2008.

[14] S. Yumeng, C. Jie, G. Caihong, S. Bing, and Z. Yinqing, "The advanced simulation system for MMW imaging radar seeker onboard air-to-air missile," in *2006 8th international Conference on Signal Processing*, pp. 1–4, Beijing, China, November 2006.

[15] Y. P. Zhang, S. X. Wang, and Y. H. Xu, "Dual-mode MMW/IR simulation of beam combiner," *Optik*, vol. 121, no. 11, pp. 1003–1008, 2010.

[16] P. Thevenon, J. Vezinet, and P. Estrade, "Estimation of the base station position error in a RTK receiver using state augmentation in a Kalman filter," in *2018 9th ESA Workshop on Satellite NavigationTechnologies and European Workshop on GNSS Signals and Signal Processing (NAVITEC)*, pp. 1–7, Noordwijk, Netherlands, December 2018.

[17] K. M. Ng, J. Johari, S. A. C. Abdullah, A. Ahmad, and B. N. Laja, "Performance evaluation of the RTK-GNSS navigating under different landscape," in *2018 18th International Conference on Control, Automation and Systems (ICCAS)*, pp. 1424–1428, Daegwallyeong, South Korea, October 2018.

[18] M. Pini, G. Marucco, G. Falco, M. Nicola, and W. De Wilde, "Experimental testbed and methodology for the assessment of RTK GNSS receivers used in precision agriculture," *IEEE Access*, vol. 8, pp. 14690–14703, 2020.

[19] G. He, M. Song, X. He, and Y. Hu, "GPS signal acquisition based on compressive sensing and modified greedy acquisition algorithm," *IEEE Access*, vol. 7, pp. 40445–40453, 2019.

[20] C. Ou, B. Wu, and L. Cai, "GPS-free vehicular localization system using roadside units with directional antennas," *Journal of Communications and Networks*, vol. 21, no. 1, pp. 12–24, 2019.

[21] X. Kong, J. Guo, and Z. Liu, *Foundation of Geodesy*, Wuhan University Press, China, 2010.

[22] E. Akeila, Z. Salcic, and A. Swain, "Reducing low-cost INS error accumulation in distance estimation using self-resetting," *IEEE Transactions on Instrumentation and Measurement*, vol. 63, no. 1, pp. 177–184, 2014.

[23] X. Zhao and Y. Kang, "Integrated navigation error analysis based on Kalman filter of INS error compensation," in *2019 3rd International Conference on Robotics and Automation Sciences (ICRAS)*, pp. 102–106, Wuhan, China, June 2019.

[24] Y. Huang, H. Yao, Y. Gao, H. Zhang, and Y. Xu, "Development of the high real-time GPS time transfer receiver," in *29th Conference on Precision Electromagnetic Measurements (CPEM 2014)*, pp. 150-151, Rio de Janeiro, Brazil, August 2014.

[25] X. Li, H. Zhang, S. Shi, and G. Wang, "Measurement of the time delay of GPS timing receiver based on UTC (NTSC)," in *2009 IEEE International Frequency Control Symposium Joint with the 22nd European Frequency and Time forum*, pp. 1073–1075, Besancon, France, April 2009.